

RADIATIVELY INEFFICIENT ACCRETION IN NEARBY GALAXIES

LUIS C. HO

The Observatories of the Carnegie Institution of Washington, 813 Santa Barbara Street, Pasadena, CA 91101, USA

To appear in The Astrophysical Journal.

ABSTRACT

We use new central stellar velocity dispersions and nuclear X-ray and H α luminosities for the Palomar survey of nearby galaxies to investigate the distribution of nuclear bolometric luminosities and Eddington ratios for their central black holes (BHs). This information helps to constrain the nature of their accretion flows and the physical drivers that control the spectral diversity of nearby active galactic nuclei. The characteristic values of the bolometric luminosities and Eddington ratios, which span over 7–8 orders of magnitude, from $L_{\text{bol}} \lesssim 10^{37}$ to 3×10^{44} erg s⁻¹ and $L_{\text{bol}}/L_{\text{Edd}} \approx 10^{-9}$ to 10^{-1} , vary systematically with nuclear spectral classification, increasing along the sequence absorption-line nuclei \rightarrow transition objects \rightarrow low-ionization nuclear emission-line regions \rightarrow Seyferts. The Eddington ratio also increases from early-type to late-type galaxies. We show that the very modest accretion rates inferred from the nuclear luminosities can be readily supplied through local mass loss from evolved stars and Bondi accretion of hot gas, without appealing to additional fueling mechanisms such as angular momentum transport on larger scales. Indeed, we argue that the fuel reservoir generated by local processes should produce far more active nuclei than is actually observed. This generic luminosity-deficit problem suggests that the radiative efficiency in these systems is much less than the canonical value of 0.1 for traditional optically thick, geometrically thin accretion disks. The observed values of $L_{\text{bol}}/L_{\text{Edd}}$, all substantially below unity, further support the hypothesis that massive BHs in most nearby galaxies reside in a low or quiescent state, sustained by accretion through a radiatively inefficient mode.

Subject headings: black hole physics — galaxies: active — galaxies: nuclei — galaxies: Seyfert

1. INTRODUCTION

Simple considerations of the quasar population predict that massive black holes (BHs) should be common in a sizable fraction of present-day galaxies. From the integrated luminosity density of quasars, one can estimate that a typical L^* galaxy should, on average, contain a waste mass of $\sim 10^7 M_{\odot}$ locked up in a BH (Soltan 1982; Chokshi & Turner 1992). But why are the quasar remnants so quiescent? Active galactic nuclei (AGNs) with quasarlike luminosities are absent at $z \approx 0$ presumably because of the diminished fuel supply currently available. For a canonical radiative efficiency of $\eta = 0.1$ appropriate for geometrically thin, optically thick accretion disks (see Frank et al. 1992), the BH has to consume 1–100 M_{\odot} yr⁻¹ in order to generate luminosities of $L_{\text{bol}} = 10^{11}$ – $10^{13} L_{\odot}$, as typically seen in quasars. This level of gas supply is difficult to sustain in nearby galaxies. On the other hand, accretion rates of $\dot{M} = 0.001$ – $0.1 M_{\odot}$ yr⁻¹ do not appear implausible. Even if angular momentum transport on nuclear scales is ineffective in disk galaxies, this level of fueling can be supplied simply through local stellar mass loss (Ho et al. 1997c). Hence, for $\eta = 0.1$, there ought to be many nuclei shining as AGNs with $L_{\text{bol}} = 10^9$ – $10^{11} L_{\odot}$. This is not observed. Only $\sim 1\%$ – 5% of galaxies contain bright Seyfert nuclei (e.g., Huchra & Burg 1992; Greene & Ho 2007a). In the case of giant elliptical galaxies experiencing cooling flows, we may expect even larger values of \dot{M} and thus correspondingly larger luminosities, again contrary to observations (Fabian & Canizares 1988).

The dilemma posed by the luminosity deficit in the nuclei of nearby elliptical galaxies can be resolved by discarding the premise that massive BHs are ubiquitous in these systems (Fabian & Canizares 1988). But this proposition is no longer tenable in light of our current knowledge on the demography of

central BHs based on direct dynamical searches (Magorrian et al. 1998; Ho 1999a; Kormendy 2004). Massive BHs appear to be a generic component of galactic structure in most, if not all, systems with a bulge. Consistent with this picture, low-level nuclear activity qualitatively resembling that of more luminous AGNs is found to be equally pervasive in nearby galaxies (Ho et al. 1997b; Ho 2008).

Radiatively inefficient accretion flows (RIAFs; see Narayan et al. 1998; Quataert 2001 for reviews) provide an attractive framework for solving the luminosity-deficit problem. In the regime when the mass accretion rate onto the central BH is very low, the low-density, optically thin accreting medium cannot cool efficiently, and the accretion flow consequently puffs up into a quasi-spherical structure. Most relevant to the present discussion, RIAFs attain radiative efficiencies much below the canonical value of 0.1. RIAFs are characteristically dim. Optically thin RIAFs are predicted to exist for accretion rates below a critical threshold of $\dot{M}_{\text{crit}} \approx \alpha^2 \dot{M}_{\text{Edd}} \approx 0.1 \dot{M}_{\text{Edd}}$ (Narayan et al. 1998), where the Eddington accretion rate is defined by $L_{\text{Edd}} = \eta \dot{M}_{\text{Edd}} c^2$, with $\eta = 0.1$ and $L_{\text{Edd}} = 1.26 \times 10^{38} (M_{\text{BH}}/M_{\odot})$ erg s⁻¹; the Shakura & Sunyaev (1973) viscosity parameter is taken to be $\alpha \approx 0.3$ (Narayan et al. 1998). Fabian & Rees (1995) and Mahadevan (1997) invoke RIAFs to explain the dimness of elliptical galaxy nuclei.

This paper discusses the luminosity-deficit problem for a large, well-defined sample of galaxies spanning a wide range of morphological types and representing all the major nuclear spectroscopic classes. We use X-ray and line luminosity measurements to constrain the accretion luminosities of the nuclei. A newly published catalog of central stellar velocity dispersions provides estimates of the BH mass through the $M_{\text{BH}}-\sigma_*$ relation (Gebhardt et al. 2000; Ferrarese & Merritt 2000). The feeble

TABLE 1
BOLOMETRIC CORRECTIONS FOR LOW-LUMINOSITY AGNs

Galaxy	Class	D_L (Mpc)	L_{bol} (erg s^{-1})	$C_{\text{H}\alpha}$			C_X	Reference
				Narrow	Broad	Total		
(1)	(2)	(3)	(4)	(5)	(6)	(7)	(8)	(9)
NGC 1097	L2/L1.9	14.5	1.8×10^{42}	529	474	250	34.4	1
NGC 3031	S1.5/L1.5	3.6	2.1×10^{41}	300	140	95	3.5	2
NGC 4203	L1.9	9.7	9.5×10^{40}	431	243	156	3.9	3
NGC 4261	L2	30.0	1.7×10^{42}	355	...	355	14.2	3
NGC 4374	L2	16.8	8.2×10^{41}	410	...	410	8.4	3
NGC 4450	L1.9	16.8	3.4×10^{41}	1064	1136	550	8.9	3
NGC 4486	L2	16.8	2.3×10^{42}	389	...	389	17.7	3
NGC 4579	S1.9/L1.9	16.8	9.9×10^{41}	353	380	184	7.7	3
NGC 4594	L2	9.2	2.7×10^{41}	208	...	208	7.5	3
NGC 6251	S2	92.0	8.0×10^{42}	36	...	36	2.9	4
Arp 102B	L1.2	96.6	2.9×10^{43}	546	62	55	1.8	5
Pictor A	L1.5	140.1	1.3×10^{44}	5000	241	228	2.7	6
			Mean	802	382	243	9.5	
			Standard Deviation	1345	360	156	9.2	
			Median	410	243	228	7.7	

NOTE.— Col. (1) Galaxy name. Col. (2) Spectroscopic classification of nucleus. Col. (3) Adopted distance. Col. (4) Bolometric luminosity. Col. (5) Ratio of bolometric to narrow $\text{H}\alpha$ luminosity. Col. (6) Ratio of bolometric to broad $\text{H}\alpha$ luminosity. Col. (7) Ratio of bolometric to total (narrow + broad) $\text{H}\alpha$ luminosity. Col. (8) Ratio of bolometric to X-ray luminosity in the 2–10 keV band. Col. (9) Reference for the $\text{H}\alpha$ data: (1) Storchi-Bergmann et al. (1993), narrow-line luminosity corrected for an extinction of $A_V = 2.46$ mag; (2) Ho et al. (1996); (3) Ho et al. (1997a); (4) Shuder & Osterbrock (1981); (5) Halpern et al. (1996); (6) Carswell et al. (1984). Data for cols. (2)–(4) and (8) come from Ho (1999b) and Ho et al. (2000).

nuclear activity in nearby galaxies can be comfortably sustained through stellar mass loss and spherical accretion of hot gas in the inner regions of bulges. We show that the inferred accretion rates lie well within the critical threshold of RIAFs. Finally, we discuss the physical connection between accretion rates and nuclear spectral types.

2. OBSERVATIONAL MATERIAL

Our analysis explicitly makes the following assumptions: (1) all galaxy bulges contain central BHs whose masses can be well estimated using the recently established correlation between BH mass and bulge stellar velocity dispersion; (2) the present level of activity of the BHs manifests itself as AGN-like emission-line nuclei; and (3) the accretion luminosity can be extrapolated through the observed nuclear X-ray or optical line luminosities.

We focus on the sample of nuclei in the Palomar survey of nearby galaxies, a magnitude-limited spectroscopic study of a nearly complete sample of 486 bright ($B_T \leq 12.5$ mag), northern ($\delta > 0^\circ$) galaxies (see Ho et al. 1997a, 1997b, and references therein). All of the galaxies have been assigned a nuclear spectroscopic classification using a set of uniform criteria, into the following classes (see Ho et al. 1997a for details): absorption-line nuclei (A), H II nuclei (H), Seyfert nuclei (S),

low-ionization nuclear emission-line regions (LINERs; L), and transition objects (T; LINER/H II composites). This paper considers all classes except the H II nuclei. The Palomar survey contains 277 galaxies classified as absorption-line (66), Seyfert (52), LINER (94), and transition nuclei (65).

2.1. Nuclear Luminosities

Our study requires bolometric luminosities for a well-defined sample of AGNs covering a wide range of power. Because AGNs emit a very broad spectrum, their bolometric luminosities ideally should be measured directly from their broadband spectral energy distributions (SEDs). In practice, however, complete SEDs are not readily available for most AGNs, least of all for low-luminosity sources such as LINERs, which are most prevalent in nearby galaxies. The largest existing compilations of broadband SEDs for low-luminosity AGNs (Ho 1999b; Ho et al. 2000; Maoz 2007) contain only a limited number of objects.

For this study, we circumvent this difficulty by using two measures of the nuclear power to estimate the AGN bolometric luminosity, one based on the $\text{H}\alpha$ emission line and another based on X-rays. Although the $\text{H}\alpha$ luminosity comprises only a small percentage of the total power, its fractional contribution to the bolometric luminosity, as shown below, turns out

to be fairly well defined. Moreover, unlike most other spectral windows, $H\alpha$ measurements are readily available for large, relatively complete samples of nuclei. The Palomar database gives $H\alpha$ luminosities measured through an aperture of $2'' \times 4''$ centered on the nucleus, which corresponds to a linear scale of $\sim 200 \text{ pc} \times 400 \text{ pc}$ for a typical distance of 20 Mpc. As explained in Ho et al. (2003a), some of the $H\alpha$ luminosities published in Ho et al. (1997a) have been updated with more accurate values from the literature. We will also make use of upper limits for the $H\alpha$ luminosity of the absorption-line nuclei that were not given explicitly in Ho et al. (1997a); the limits were calculated from the equivalent-width detection limit of the survey in conjunction with the 6600 \AA continuum flux density measurements, assuming that the line has a typical full width at half-maximum (FWHM) of 250 km s^{-1} . A supplementary list of $H\alpha$ luminosities, including the upper limits, is given in Ho et al. (2003a). In total, $H\alpha$ luminosities, or upper limits thereof, are available for 246 objects, which account for 80%, 98%, 89%, and 91% of the nuclear classes A, S, L, and T, respectively. Thus, $H\alpha$ measurements are available for the vast majority of the objects considered in this study.

The bolometric correction for $H\alpha$, $C_{H\alpha} = L_{\text{bol}}/L_{H\alpha}$, can be obtained in one of two ways. For luminous, type 1 AGNs, it is often expedient to estimate L_{bol} from the optical continuum luminosity, frequently chosen at 5100 \AA in the recent literature: $L_{\text{bol}} = C_{5100} \lambda L_{\lambda}(5100)$. Now, the $H\alpha$ luminosity correlates strongly with the optical continuum, including $\lambda L_{\lambda}(5100)$ (Greene & Ho 2005); the correlation is slightly nonlinear. Choosing $C_{5100} = 9.8$ (McLure & Dunlop 2004), Greene & Ho (2007a) obtain $L_{\text{bol}} = 2.34 \times 10^{44} (L_{H\alpha}/10^{42} \text{ erg s}^{-1})^{0.86} \text{ erg s}^{-1}$. The conversion pertains to the entire $H\alpha$ line, which in luminous type 1 AGNs is dominated by the broad component. Because of the reliance on the $L_{H\alpha} - \lambda L_{\lambda}(5100)$ correlation and the assumption that C_{5100} is constant, the relation between L_{bol} and $L_{H\alpha}$ is formally slightly nonlinear. It is unclear how robust this result is and whether it can be extrapolated toward lower luminosities. For the luminosity range of interest to us, it introduces an uncertainty of a factor of ~ 2 into the bolometric correction. For $L_{H\alpha} = 10^{38}$, 10^{39} , and $10^{40} \text{ erg s}^{-1}$, $C_{H\alpha} \approx 850$, 615, and 446, respectively.

Alternatively, we can attempt to estimate $C_{H\alpha}$ empirically from the observed SEDs of low-luminosity AGNs, limited though they may be. We use the sample of 12 low-luminosity Seyferts and LINERs with broadband SEDs studied by Ho (1999b) and Ho et al. (2000; see also Ho 2002b) as a guide. The data, summarized in Table 1, show that the median value of $C_{H\alpha}$ ranges from 228 to 410, depending on whether we include only the narrow component of the line, only the broad component, or both. A reasonable compromise might be $C_{H\alpha} \approx 300 \pm 100$. Preliminary analysis of a more extensive sample of SEDs (L. C. Ho, in preparation) shows that the bolometric correction for the $H\beta$ line has a significant scatter, especially for low-luminosity sources. For sources with Eddington ratios below 0.1, and assuming that on average $H\alpha/H\beta = 3.5$ (Greene & Ho 2005), the median value of $C_{H\alpha} \approx 220$ with an interquartile range of 160. This agrees reasonably well with the range of values obtained from our calibration sample in Table 1. For concreteness, we will simply adopt $C_{H\alpha} = 300$; none of the main conclusions in this study depends critically on the exact value of the bolometric correction.

The $H\alpha$ luminosities of the narrow-line objects are subject to a potential source of complication. From consideration of

the relative strength of X-ray (2–10 keV) and $H\alpha$ emission in different classes of nearby AGNs, Ho (2008) shows that type 2 sources (Seyfert 2s, LINER 2s, and essentially all of the transition objects) have a general tendency to emit excess optical line emission compared to their type 1 counterparts. He attributes this excess emission to extranuclear processes unassociated with the active nucleus. If this interpretation is correct, then only a fraction of the narrow $H\alpha$ emission should be included in the budget for the nuclear luminosity. Ho (2008) finds that the median ratio of $L_X/L_{H\alpha}$ is 7.3 for Seyfert 1s and 4.6 for LINER 1s, whereas Seyfert 2s, LINER 2s, and transition objects have significantly lower values of 0.75, 1.6, and 0.41, respectively. Assuming, for concreteness, that the intrinsic $L_X/L_{H\alpha}$ ratio for the type 2 sources is equal to that of LINER 1s, the $H\alpha$ luminosities for Seyfert 2s, LINER 2s, and transition objects need to be reduced by a factor of 6.1, 2.9, and 11.2, respectively.

In light of the above source of ambiguity with the $H\alpha$ emission, it would be desirable to have an alternative handle on the nuclear luminosity. By far the most secure measure of nuclear luminosity in AGNs comes from X-ray observations. Because of the faintness of low-luminosity AGNs, the data must be of high enough angular resolution so that the nucleus can be cleanly separated from the host galaxy (e.g., Ho et al. 2001; Flohic et al. 2006). As reviewed in Ho (2008), a substantial fraction of the galaxies in the Palomar survey have now been observed in the X-rays. The Appendix gives a compilation of all pertinent X-ray measurements taken from the literature, as well as from new analysis of data taken from the *Chandra* public archives. The X-ray data are not nearly as complete as $H\alpha$. Nevertheless, X-ray luminosities, or upper limits thereof, are now available for 175 out of the 277 objects in the parent sample (63%), which account for 47% of the absorption nuclei, 68% of the LINERs, 83% of the Seyferts, and 57% of the transition objects. The incompleteness and heterogeneous nature of the X-ray measurements make it difficult to rigorously assess selection effects. However, if observational biases exist, they should be in the direction of missing very faint sources, an effect that strengthens our main conclusions.

As with the $H\alpha$ data, determining the appropriate bolometric correction for the X-ray band is not trivial. Since the SEDs of AGNs vary strongly with accretion rate (Ho 1999b), we must abandon the usual practice of adopting a single correction factor based on the average SED of luminous quasars. Using, again, the small sample of low-luminosity AGNs with reliable broadband SEDs, Table 1 shows that the median value of the bolometric correction in the 2–10 keV band is $C_X = L_{\text{bol}}/L_X \approx 8$, where L_X is the luminosity in the 2–10 keV band, corrected, to the extent possible, for absorption. The more extensive data set of L. C. Ho (in preparation) suggests a value larger by about a factor of 2: sources with $L_{\text{bol}}/L_{\text{Edd}} \lesssim 0.1$ have a median $C_X = 15.8$, with an interquartile range of 9.6. Because low-luminosity AGNs tend to be “X-ray-loud” (Ho 1999b) their values of C_X are significantly smaller than conventionally assumed for luminous sources ($C_X \approx 35$; Elvis et al. 1994). This is consistent with the analysis of Vasudevan & Fabian (2007). For the present purposes, we will adopt $C_X = 15.8$, noting, as before, that factors of a few variation in the bolometric correction do not affect the main conclusions of this study.

The uncertainties on L_{bol} are difficult to estimate. As discussed in Ho et al. (1997a), the $H\alpha$ fluxes in the Palomar survey have typical errors of 30%–50%, reaching 100% in the worst

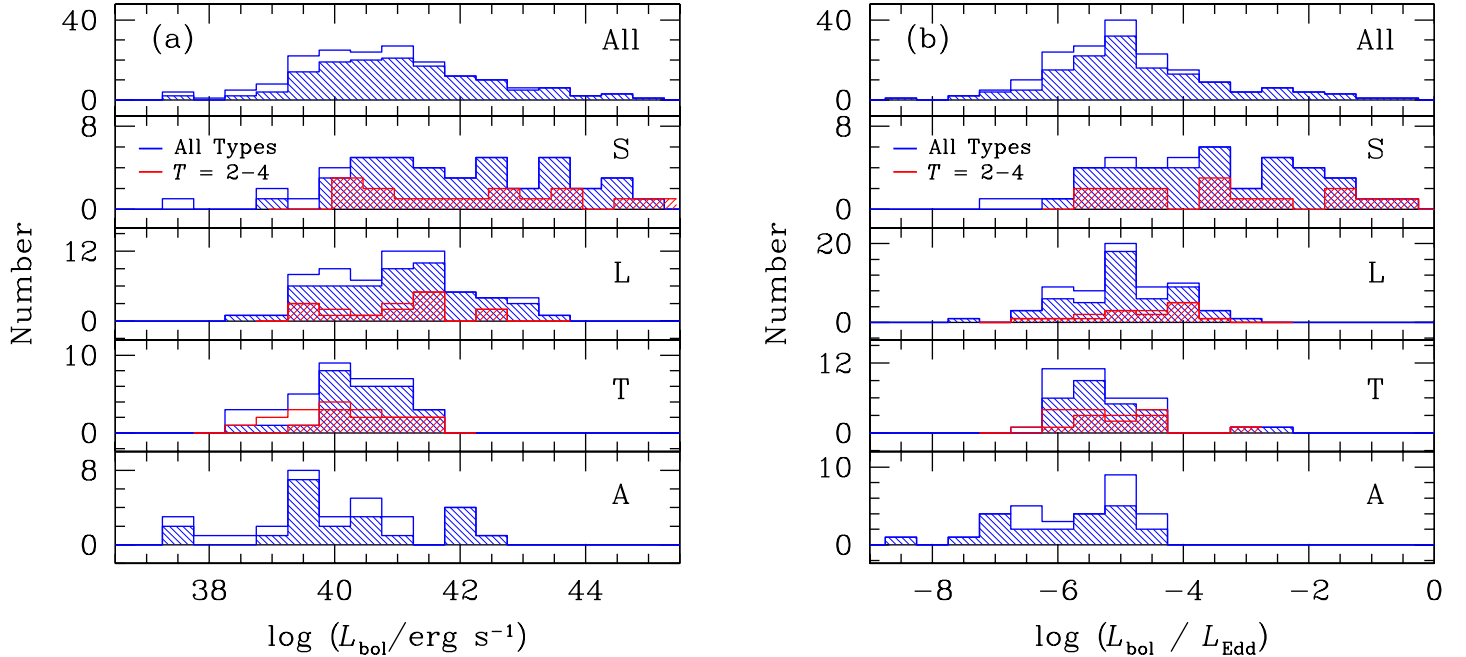


FIG. 1.— Distribution of (a) bolometric luminosity, L_{bol} , and (b) ratio of bolometric luminosity to the Eddington luminosity, $L_{\text{bol}}/L_{\text{Edd}}$, for all objects, Seyferts (L), LINERs (L), transition nuclei (T), and absorption-line nuclei (A). The hatched and open histograms denote detections and upper limits, respectively. The original sample is shown in blue, and the subsample restricted to Sab–Sbc ($T = 2-4$) Hubble types is shown in red. The bolometric luminosity is based on the 2–10 keV X-ray luminosity, assuming $L_{\text{bol}} = 15.8L_X$.

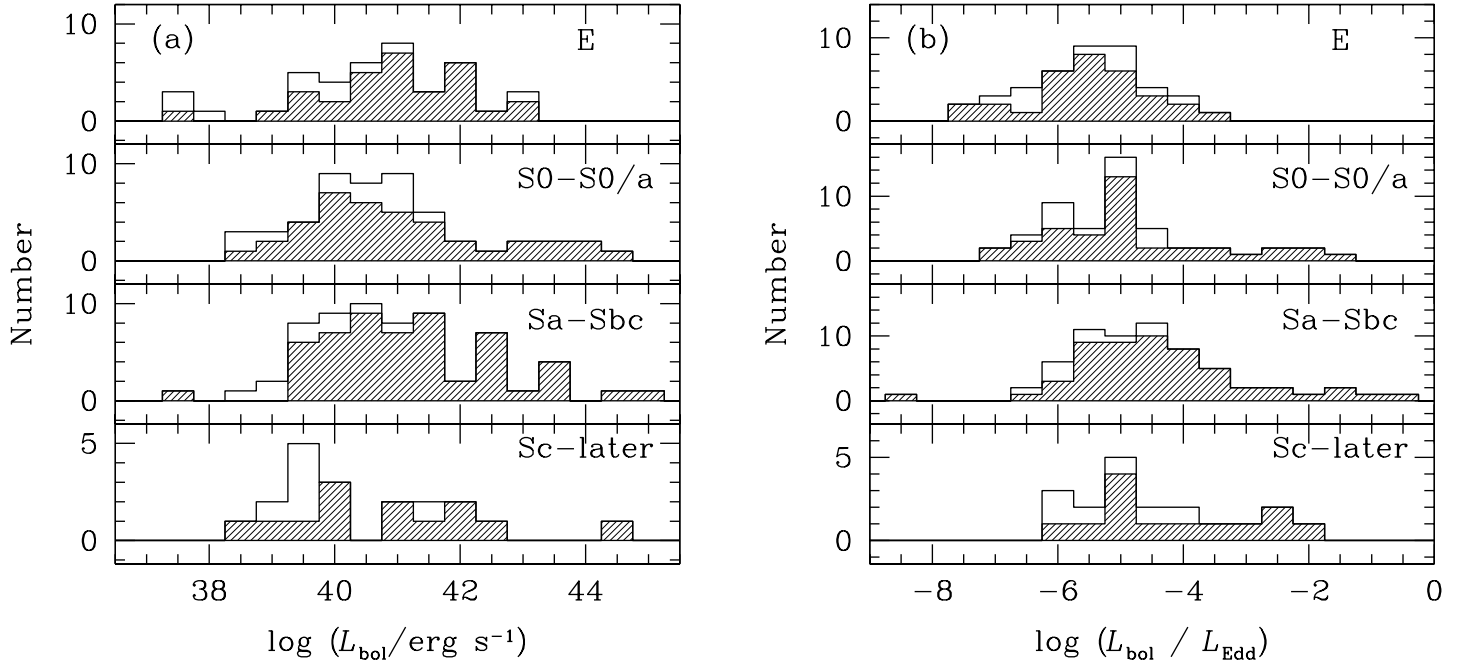


FIG. 2.— Distribution of (a) bolometric luminosity, L_{bol} , and (b) ratio of bolometric luminosity to the Eddington luminosity, $L_{\text{bol}}/L_{\text{Edd}}$, for galaxies binned by Hubble type. The hatched and open histograms denote detections and upper limits, respectively. The bolometric luminosity is based on the 2–10 keV X-ray luminosity, assuming $L_{\text{bol}} = 15.8L_X$.

cases. The largest source of uncertainty for the $H\alpha$ -based luminosities, however, comes from our still-tentative knowledge of $C_{H\alpha}$ (factor ~ 2) and the amount of extranuclear contamination of the narrow-line emission (factor $\sim 2-5$, depending on the spectral class). In the X-ray band, we can be more confident that the flux is largely nuclear, and large-amplitude variability

seems to be rather uncommon for the systems in question (Ho 2008). Not all of the X-ray detections have sufficient counts for rigorous spectral fitting, but fortunately low-luminosity AGNs generally have small absorbing columns (Ho 2008). Still, at the moment we do not know C_X to better than a factor of ~ 2 . We conservatively guess that the estimates of L_{bol} based on $H\alpha$

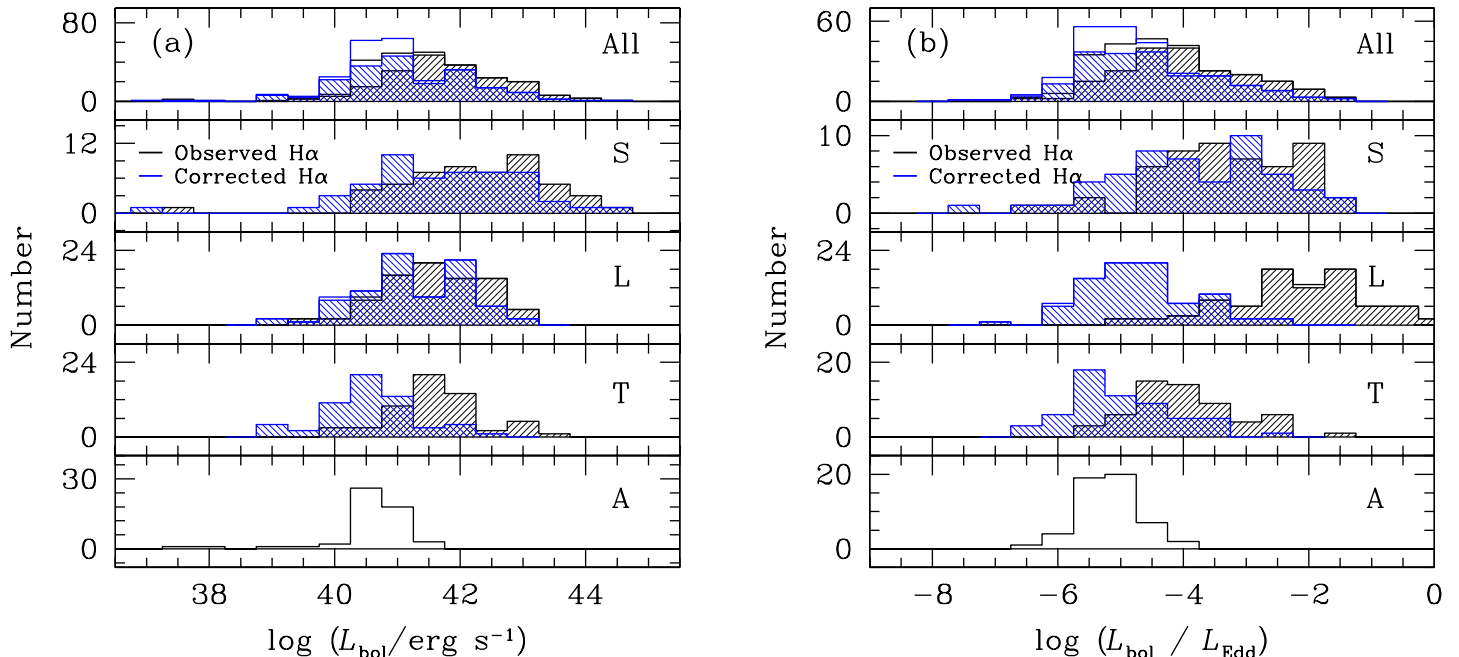


FIG. 3.— Distribution of (a) bolometric luminosity, L_{bol} , and (b) ratio of bolometric luminosity to the Eddington luminosity, $L_{\text{bol}}/L_{\text{Edd}}$, for all objects, Seyferts (L), LINERs (L), transition nuclei (T), and absorption-line nuclei (A). The bolometric luminosity is based on the extinction corrected total (narrow + broad) H α luminosity, assuming $L_{\text{bol}} = 300L_{\text{H}\alpha}$. The blue histograms show the distributions after correcting the narrow-line sources for extranuclear contamination (see text for details). The hatched and open histograms denote detections and upper limits, respectively.

and X-rays measurements have uncertainties of 0.7 and 0.3 dex, respectively.

2.2. Black Hole Masses

The majority of the objects in our sample do not have direct, dynamically determined BH masses. We will estimate BH masses using the tight correlation between BH mass and bulge stellar velocity dispersion (the $M_{\text{BH}}-\sigma_*$ relation: Gebhardt et al. 2000; Ferrarese & Merritt 2000), as determined by Tremaine et al. (2002):

$$\log\left(\frac{M_{\text{BH}}}{M_{\odot}}\right) = (4.02 \pm 0.32) \log\left(\frac{\sigma_*}{200 \text{ km s}^{-1}}\right) + (8.13 \pm 0.06). \quad (1)$$

The intrinsic scatter of the above fit is estimated to be $\lesssim 0.3$ dex. The fit uses σ_e , the luminosity-weighted velocity dispersion measured within the effective radius of the bulge. Since we do not have measurements of σ_e for most of our galaxies, we use instead σ_0 , the central velocity dispersion. Gebhardt et al. (2000) have shown that in general $\sigma_0 \approx \sigma_e$ within a scatter of $\sim 10\%$.

Ho et al. (2009) recently published a comprehensive, uniform catalog of central velocity dispersions for nearly all of the galaxies in the Palomar survey. New stellar velocity dispersions were obtained for a total of 428 galaxies, and estimates for another 34 were obtained indirectly from the line width of [N II] $\lambda 6583$ using the calibration of Ho (2009). The typical uncertainties in the velocity dispersions range from $\sim 5\%$ to 15% . An error of 10% in σ_* introduces an uncertainty of ~ 0.15 dex in $\log M_{\text{BH}}$. We assume that M_{BH} has an uncertainty dominated by the scatter of the $M_{\text{BH}}-\sigma_*$ relation, ~ 0.3 dex.

3. BOLOMETRIC LUMINOSITIES AND EDDINGTON RATIOS

Figure 1 shows the distributions of bolometric luminosities and their values normalized with respect to the Eddington luminosity, $L_{\text{bol}}/L_{\text{Edd}}$. To avoid the possible complication of extranuclear contamination in the H α emission, we base the bolometric luminosities on the hard X-ray measurements. The statistics of the distributions are listed in Table 2. The four classes of nuclei comprise a sequence of increasing luminosity: A \rightarrow T \rightarrow L \rightarrow S. Whereas LINER and transition nuclei have very similar H α luminosities (Ho et al. 2003a)—an effect that can be attributed to the H α emission in transition objects being boosted by non-nuclear sources (Ho 2008)—there is no doubt that in the hard X-ray band LINERs are more luminous than transition objects (median $L_{\text{bol}} = 3.0 \times 10^{40}$ vs. 6.5×10^{39} erg s $^{-1}$). Both LINERs and transition objects, in turn, are less powerful than Seyferts (median $L_{\text{bol}} = 2.2 \times 10^{41}$ erg s $^{-1}$). This systematic trend becomes even more sharply defined when we consider the Eddington ratios. As with L_{bol} , the median value of $L_{\text{bol}}/L_{\text{Edd}}$ for LINERs (6.0×10^{-6}) is a factor of 4 larger than for transition objects (1.5×10^{-6}), both being 1–2 orders of magnitude smaller than in Seyferts (1.1×10^{-4}). Notably, *all* galactic nuclei in the Palomar sample are highly sub-Eddington systems.

The distribution of L_{bol} is broadly similar for galaxies of different morphological types (Fig. 2a). By contrast, $L_{\text{bol}}/L_{\text{Edd}}$ increases mildly, but systematically, from early-type to late-type galaxies (Fig. 2b). Since the various classes of emission-line nuclei in the Palomar survey are hosted by slightly different Hubble types (Ho et al. 2003a), it would be of interest to examine the trends in L_{bol} and $L_{\text{bol}}/L_{\text{Edd}}$ after factoring out the dependence on Hubble type. This is illustrated by the red histograms in Figure 1, where we now restrict the comparison to galaxies with morphological types Sab–Sbc ($T = 2-4$), a subset that, as shown in Ho et al. (2003a), has statistically identical

TABLE 2
SAMPLE STATISTICS^a

Sample	N	N_u	L_{bol} (erg s ⁻¹)			$L_{\text{bol}}/L_{\text{Edd}}$		
			Mean	Error	Median	Mean	Error	Median
All (all types)	175	37	8.5×10^{42}	4.2×10^{42}	2.0×10^{40}	2.3×10^{-3}	1.2×10^{-3}	4.0×10^{-6}
S (all types)	43	3	3.4×10^{43}	1.7×10^{43}	2.2×10^{41}	9.2×10^{-3}	4.9×10^{-3}	1.1×10^{-4}
(Sab-Sbc)	15	0	5.9×10^{43}	4.3×10^{43}	7.2×10^{41}	2.3×10^{-2}	1.3×10^{-2}	2.5×10^{-4}
L (all types)	64	12	6.1×10^{41}	2.3×10^{41}	3.0×10^{40}	3.0×10^{-5}	1.0×10^{-5}	6.0×10^{-6}
(Sab-Sbc)	16	2	1.9×10^{41}	8.9×10^{40}	8.3×10^{40}	3.3×10^{-5}	1.2×10^{-5}	6.9×10^{-6}
T (all types)	37	10	3.0×10^{40}	9.7×10^{39}	6.5×10^{39}	5.1×10^{-5}	3.7×10^{-5}	1.5×10^{-6}
(Sab-Sbc)	17	6	3.5×10^{40}	1.8×10^{40}	3.4×10^{39}	3.1×10^{-5}	2.5×10^{-5}	1.9×10^{-6}
A (all types)	31	10	1.3×10^{41}	5.8×10^{40}	1.8×10^{39}	3.1×10^{-6}	1.0×10^{-6}	2.2×10^{-7}
E	41	10	4.6×10^{41}	2.0×10^{41}	1.7×10^{40}	1.2×10^{-5}	5.8×10^{-6}	1.2×10^{-6}
S0-S0/a	51	12	8.1×10^{42}	5.3×10^{42}	1.2×10^{40}	7.1×10^{-4}	4.7×10^{-4}	4.7×10^{-6}
Sa-Sbc	64	9	1.5×10^{43}	1.1×10^{43}	3.1×10^{40}	5.5×10^{-3}	3.3×10^{-3}	9.2×10^{-6}
Sc-later	19	6	6.1×10^{42}	5.7×10^{42}	3.6×10^{39}	5.9×10^{-4}	3.7×10^{-4}	4.2×10^{-6}

^aThe bolometric luminosities are based on the 2–10 keV X-ray luminosity, assuming $L_{\text{bol}} = 15.8L_X$. Statistics for subsamples containing upper limits (whose number is denoted by N_u) computed using the Kaplan-Meier product-limit estimator (Feigelson & Nelson 1985). Our sample contains four galaxies (NGC 1275, 4261, 4374, and 4486) with strong FR I-type (Fanaroff & Riley 1974) radio jets, as noted in Table 3. The nuclear X-ray luminosities of these objects might be partly contaminated by emission from the jet component. Excluding these four galaxies does not significantly change the statistics of this table.

distributions of morphological types for all three AGN subclasses. The overall trends of the parent sample are preserved (see also Table 2).

Although in this study we give preference to the X-ray luminosities over the $H\alpha$ luminosities because of concerns over extranuclear line contamination, the $H\alpha$ data have the advantage of being uniform and nearly complete. Figure 3 repeats the analysis of Figure 1, but now using bolometric luminosities derived from $H\alpha$. The black histograms show the $H\alpha$ luminosities as observed, converted to L_{bol} assuming a bolometric correction of $C_{H\alpha} = 300$. The blue histograms plot the same data with a statistical correction for extranuclear line emission applied to the Seyfert 2s, LINER 2s, and transition objects based on their observed $L_X/L_{H\alpha}$ ratio (see § 2.1). Not surprisingly, the overall trends seen in Figure 1 are well mirrored in Figure 3, but now they are delineated with better statistics.

Finally, we turn to the distribution of M_{BH} and L_{bol} vs. $L_{\text{bol}}/L_{\text{Edd}}$ (Fig. 4). In these diagrams, we have marked the various subclasses of nuclei, and we have included the large sample of $z < 0.35$ high-luminosity AGNs (Seyfert 1 nuclei and low-redshift quasars) selected by Greene & Ho (2007a) from the Sloan Digital Sky Survey (SDSS). Greene & Ho derived BH masses and bolometric luminosities using the width and strength of the broad $H\alpha$ line. We point out several salient features.

1. Considered collectively, there is no dependence of M_{BH} on $L_{\text{bol}}/L_{\text{Edd}}$: at a given value of M_{BH} , which mostly fall in the range $10^6 - 10^9 M_{\odot}$, $L_{\text{bol}}/L_{\text{Edd}}$ spans ~ 6 orders of magnitude within the Palomar sample and ~ 8 orders of magnitude if the sample of luminous sources is included.
2. Within each class of emission-line objects, especially among LINERs and transition nuclei, there is a loose

inverse correlation between M_{BH} and $L_{\text{bol}}/L_{\text{Edd}}$. This arises because L_{bol} spans a narrower range of values than M_{BH} .

3. At a fixed value of M_{BH} , $L_{\text{bol}}/L_{\text{Edd}}$ increases systematically along the sequence absorption-line nuclei \rightarrow transition objects \rightarrow LINERs \rightarrow low-luminosity Seyferts \rightarrow high-luminosity Seyferts and quasars. There is considerable overlap among the classes. The apparent gap in $L_{\text{bol}}/L_{\text{Edd}}$ between the Palomar and SDSS sample may be an artifact of observational selection effects; the two surveys have very different sensitivity limits (Ho 2008).
4. All emission-line nuclei in nearby galaxies are sub-Eddington systems, with the vast majority having $L_{\text{bol}}/L_{\text{Edd}} \ll 1$. All LINERs and transition nuclei are characterized by $L_{\text{bol}}/L_{\text{Edd}} < 10^{-2}$.
5. The combined distribution of L_{bol} or $L_{\text{bol}}/L_{\text{Edd}}$ for the Palomar sample shows no evidence for bimodality or other indications of an abrupt transition between low-ionization (LINERs and transition objects) and high-ionization (Seyferts) sources.
6. Because L_{bol} spans a much larger range than M_{BH} , L_{bol} broadly increases with increasing $L_{\text{bol}}/L_{\text{Edd}}$. Low luminosity generally corresponds to low Eddington ratios. But there are important exceptions. A minority of AGNs have low luminosities because they have low BH masses, not necessarily low Eddington ratios. Within the Palomar sample, NGC 4395 (Filippenko & Ho 2003) provides a good example (Fig. 4b), and similar types of low-mass AGNs have been discovered in SDSS (Greene & Ho 2004, 2007b).

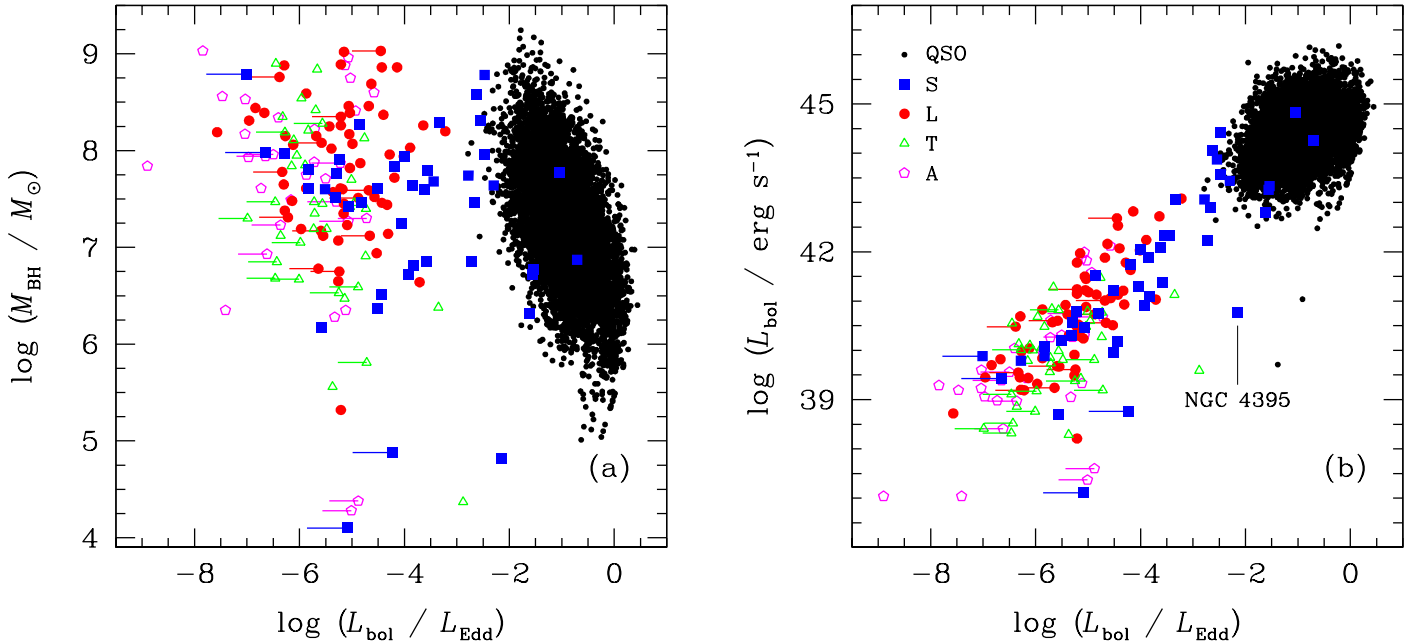


FIG. 4.— Distribution of (a) BH masses and (b) L_{bol} vs. $L_{\text{bol}}/L_{\text{Edd}}$ for objects separated by spectral classification. The bolometric luminosity is based on the 2–10 keV X-ray luminosity, assuming $L_{\text{bol}} = 15.8L_X$. The symbols are identified in the legend. The objects marked as “QSO” refer to the sample of high-luminosity Seyfert 1 nuclei and quasars studied by Greene & Ho (2007a). Line segments denote upper limits.

4. SOURCES OF FUEL

In this section we make some rough estimates of the *minimum* amount of fuel likely to be available in the central regions of nearby galaxies. For the moment, let us neglect any contribution due to dissipation from a large-scale disk, external acquisition from tidal interactions and infall, or to discrete, episodic events such as tidal disruptions of stars. Galactic nuclei can be fed, in a steady state manner from the inner bulge of the galaxy, by at least two sources: (1) ordinary mass loss from evolved stars and (2) gravitational capture of gas from the hot interstellar medium.

4.1. Stellar Mass Loss

Present-day elliptical galaxies and the bulges of S0s and spirals contain mostly old, evolved stars. Red giants and planetary nebulae return a significant fraction of their mass to the interstellar medium through mass loss. For a Salpeter stellar initial mass function with a lower mass cutoff of $0.1 M_{\odot}$, an upper mass cutoff of $100 M_{\odot}$, solar metallicities, and an age of 15 Gyr, Padovani & Matteucci (1993) estimate

$$\dot{M}_* \approx 3 \times 10^{-11} \left(\frac{L}{L_{\odot,V}} \right) M_{\odot} \text{ yr}^{-1}. \quad (2)$$

This result is consistent, within a factor of ~ 2 , with the work of Faber & Gallagher (1976), Ciotti et al. (1991), and Jungwiert et al. (2001). Athey et al. (2002) obtained mid-infrared observations to probe more directly the mass-losing stars in elliptical galaxies. They find $\dot{M}_* \approx 7 \times 10^{-12} (L/L_{\odot,B}) M_{\odot} \text{ yr}^{-1}$. For $B-V \approx 1$ mag, appropriate for an evolved population (e.g., Fukugita et al. 1995), $\dot{M}_* \approx 2 \times 10^{-11} (L/L_{\odot,V}) M_{\odot} \text{ yr}^{-1}$, again close to the estimate by Padovani & Matteucci (1993). Thus, we use Padovani & Matteucci’s relation to convert between V -band luminosity and mass loss rate.

Hubble Space Telescope (HST) images have offered an unprecedentedly detailed view of the morphological structure of the central regions of nearby galaxies. The majority of galaxies contain central density concentrations, either in the form of nuclear cusps or photometrically distinct, compact stellar nuclei (e.g., Lauer et al. 1995; Phillips et al. 1996; Carollo et al. 1997; Faber et al. 1997; Rest et al. 2001; Ravindranath et al. 2001; Böker et al. 2002; Ferrarese et al. 2006; Kormendy et al. 2009). The cusp profiles continue to rise to the resolution limit of *HST* ($0''.1$), which is ~ 10 pc at a distance of 20 Mpc. The nuclear stellar population in most instances is old (Ho et al. 2003a; Sarzi et al. 2005; Zhang et al. 2008). How much gaseous material is available through stellar mass loss? We note that the uncertainties associated with the effectiveness of angular momentum transport on large (1–10 kpc) or intermediate (0.1–1 kpc) scales are bypassed by focusing only on *nuclear* ($\lesssim 10$ pc) scales. Although the fate of the nuclear gas is not entirely clear, it is important to recognize that stellar mass loss confined to the nuclear cusp or nuclear cluster does furnish a steady state, *in situ* supply of gas that is in principle available for accretion. Shortly after being shed, the stellar gaseous envelopes quickly become thermalized with the hot ambient medium of the bulge, but some of the gas remains cool (Parriott & Bregman 2008). Even after the stellar ejecta joins the hot phase, the cooling time is sufficiently short in the inner region of the bulge that a cooling flow should develop (Mathews 1990).

The three main Local Group galaxies (M31, M32, and M33) serve as instructive examples. From the work of Lauer et al. (1998), the central stellar densities of all three galaxies rise steeply toward the center as $\rho \propto r^{-1.5 \pm 0.5}$; at $r = 0.1$ pc, the density reaches $\rho \approx 10^{6.5 \pm 0.3} M_{\odot} \text{ pc}^{-3}$. More typically, for galaxies beyond the Local Group, *HST* data probe $r \approx 10$ pc, where $\rho \approx 10 - 10^3 L_{\odot,V} \text{ pc}^{-3}$ for the “core” ellipticals and $\rho \approx 10^2 - 10^4 L_{\odot,V} \text{ pc}^{-3}$ for the “power-law” ellipticals and bulges of early-type spirals and S0s (e.g., Faber

et al. 1997). Within a spherical region of $r = 10$ pc, the diffuse cores have $L \approx 4 \times 10^4 - 4 \times 10^6 L_{\odot, V}$, which yields $\dot{M}_* \approx 1 \times 10^{-6} - 1 \times 10^{-4} M_{\odot} \text{ yr}^{-1}$; for the denser power-law cusps, $L \approx 4 \times 10^5 - 4 \times 10^7 L_{\odot, V}$, or $\dot{M}_* \approx 1 \times 10^{-5} - 1 \times 10^{-3} M_{\odot} \text{ yr}^{-1}$. Centrally dominant nuclear star clusters, present in a large fraction of disk galaxies, typically have luminosities $L \approx 10^7 L_{\odot}$ (Lauer et al. 1995; Carollo et al. 1997; Böker et al. 2002), and hence $\dot{M}_* \approx 10^{-3} M_{\odot} \text{ yr}^{-1}$.

4.2. Bondi Accretion

The inner regions of ellipticals and bulges contain X-ray-emitting plasma, sustained through thermalized ejecta from stellar mass loss (Mathews 1990), with temperatures characteristic of the virial velocities of the stars, $\sim 10^6 - 10^7$ K. This diffuse, hot gas holds another plentiful fuel reservoir for accretion, through the mechanism described by Bondi (1952). The Bondi accretion rate depends on the gas density and temperature at the accretion radius, $R_a \approx GM/c_s^2$, where $c_s \approx 0.1 T^{1/2} \text{ km s}^{-1}$ is the sound speed of the gas. From the continuity equation, $\dot{M}_B = 4\pi R_a^2 \rho_a c_s$, where ρ_a is the gas density at R_a . Expressed in terms of typical observed parameters (see below),

$$\dot{M}_B \approx 7.3 \times 10^{-4} \left(\frac{M_{\text{BH}}}{10^8 M_{\odot}} \right)^2 \left(\frac{n}{0.1 \text{ cm}^{-3}} \right) \left(\frac{200 \text{ km s}^{-1}}{c_s} \right)^3 M_{\odot} \text{ yr}^{-1} \quad (3)$$

Recent high-resolution X-ray observations using *Chandra* find that the diffuse gas in the central few hundred parsec regions of elliptical galaxies typically has temperatures of $kT \approx 0.3 - 1$ keV and densities of $n \approx 0.1 - 0.3 \text{ cm}^{-3}$ (Di Matteo et al. 2001; Loewenstein et al. 2001; Sarazin et al. 2000; Pellegrini 2005; Soria et al. 2006). Data for the bulges of spiral and S0 galaxies are more fragmentary. *Chandra* has so far resolved the hot gas in the centers of a handful of bulges, including the Milky Way (Sbc; Baganoff et al. 2003), M81 (Sab; Swartz et al. 2003), NGC 1291 (Sa; Irwin et al. 2002), and NGC 1553 (S0; Blanton et al. 2001). The center of M31 (Sb) has been investigated using both *XMM-Newton* (Shirey et al. 2001) and *Chandra* (Garcia et al. 2005). These studies suggest that bulges typically have gas temperatures of $kT \approx 0.3 - 0.5$ keV. Information on gas densities is sketchier, but judging from the work on M81 and NGC 1291, a fiducial value might be $n \approx 0.1 \text{ cm}^{-3}$.

If, for simplicity, we assume that the hot gas in most bulges is characterized by $n = 0.1 \text{ cm}^{-3}$ and $kT = 0.3$ keV, then $\dot{M}_B \approx 10^{-5} - 10^{-3} M_{\odot} \text{ yr}^{-1}$ for $M_{\text{BH}} = 10^7 - 10^8 M_{\odot}$. In elliptical galaxies $M_{\text{BH}} \approx 10^8 - 10^9 M_{\odot}$, and for $n = 0.2 \text{ cm}^{-3}$ and $kT = 0.5$ keV, $\dot{M}_B \approx 10^{-4} - 10^{-2} M_{\odot} \text{ yr}^{-1}$. We note that these estimates of the Bondi accretion rates are probably lower limits because the actual densities near R_a are likely to be higher than we assumed. For the above fiducial temperatures and BH masses, $R_a \approx 1 - 10$ pc for bulges and $\sim 10 - 100$ pc for ellipticals, roughly an order of magnitude smaller than the typical linear resolution achieved by *Chandra* for nearby galaxies. In the case of the Galactic center, $n = 26 \text{ cm}^{-3}$ and $kT = 1.3$ keV at $10''$ (0.4 pc), rising to $n = 130 \text{ cm}^{-3}$ and $kT = 2$ keV at $1''$ (Baganoff et al. 2003).

4.3. Other Sources

¹As originally formulated by Narayan & Yi (1994, 1995), this class of accretion disk models was called advection-dominated accretion flows. Subsequent work has shown that such flows are inherently unstable to outflows and convection. To avoid delving into the technical details, which are unimportant for the present level of discussion, we simply follow Quataert (2001) and refer to this class of models as RIAFs.

The two processes discussed above—ordinary stellar mass loss and Bondi accretion of hot gas—can be regarded as a conservative, steady state supply of fuel for galactic nuclei. Other sources, however, can raise this minimum level. In terms of purely stellar sources, some possibilities include (1) stellar mass loss enhanced by dynamical heating (Allen & Hughes 1987; Armitage et al. 1996) or AGN irradiation (Edwards 1980; Scoville & Norman 1988; Voit & Shull 1988), (2) stellar-stellar collisions in a dense nuclear cluster (Spitzer & Saslaw 1966; Frank 1978; Rauch 1999), and (3) tidal disruption of stars by the central BH (Hills 1975; Rees 1988; Milosavljević et al. 2006). It is difficult to evaluate quantitatively the contribution these effects would make to the total fuel budget of nearby nuclei; we merely note that cumulatively they may significantly boost the “baseline” accretion rate estimated above.

We have also neglected any contribution from the cold phase of the interstellar medium. Nonaxisymmetric perturbations due to galaxy-galaxy tidal interactions, large-scale bars, nuclear bars, or nuclear spirals are often invoked as mechanisms for angular momentum transport of the cold gas in disk galaxies (e.g., Wada 2004). The effectiveness of these processes for fueling nearby, relatively low-luminosity AGNs, however, has been unclear. With respect to the well-studied Palomar survey, AGN activity seems to be affected neither by large-scale bars (Ho et al. 1997c) nor by local galaxy environment (Schmitt 2001; Ho et al. 2003a). In any event, if dissipation of the cold gas does occur on nuclear scales, as inevitably it must at some level in at least some objects, it would further add to the fuel supply.

5. IMPLICATIONS

5.1. Accretion Flow and Radiative Efficiency

The results presented in this paper provide some important insights into the nature of BH accretion in nearby galactic nuclei. We have established, for the first time using a large, statistically robust sample, that virtually *all* massive BHs in the nearby Universe share two common properties: they have low luminosities and radiate well below the Eddington limit. This holds for galaxies spanning a wide range of Hubble types and nuclear spectral classes. The median value of the bolometric luminosities are only $L_{\text{bol}} \approx 10^{39} - 10^{41} \text{ erg s}^{-1}$, and the median Eddington ratios range from $L_{\text{bol}}/L_{\text{Edd}} \approx 2 \times 10^{-7}$ to 3×10^{-4} .

The extreme dimness of these nuclei strongly suggests that their accretion flows are radiatively inefficient. In the context of the class of accretion models commonly called optically thin RIAFs¹ the accretion luminosity is given by (Mahadevan 1997) $L_{\text{acc}} = (\eta/0.1) [0.20(\dot{m}/\alpha^2)] \dot{M} c^2$, valid in the regime $\dot{m} > 10^{-3} \alpha^2$, where $\dot{M} = \dot{m} \dot{M}_{\text{Edd}}$ and $\dot{M}_{\text{Edd}} = 2.2 \times 10^{-8} (\eta/0.1) (M_{\text{BH}}/M_{\odot}) M_{\odot} \text{ yr}^{-1}$. This expression adopts the canonical values of the microphysics parameters used by Mahadevan (1997). In the notation used in this paper,

$$\dot{m} \simeq 0.7 \left(\frac{\alpha}{0.3} \right) \left(\frac{L_{\text{bol}}}{L_{\text{Edd}}} \right)^{1/2}. \quad (4)$$

Thus, for $L_{\text{bol}}/L_{\text{Edd}} = 10^{-6} - 10^{-4}$, $\dot{m} \approx 3 \times 10^{-4} - 2 \times 10^{-2}$, which lie comfortably within the regime of optically thin RIAFs, $\dot{m} \leq \dot{m}_{\text{crit}} \approx \alpha^2 \approx 0.1$ (Narayan et al. 1998). The corresponding absolute mass accretion rates, for $M_{\text{BH}} \approx 10^6 - 10^9 M_{\odot}$, are $\dot{M} \approx 10^{-5} - 10^{-1} M_{\odot} \text{ yr}^{-1}$.

The accretion rates estimated in § 4 provide a more direct argument that the radiative efficiency of the accretion flow, whatever its form, is likely to be low. The median bolometric luminosities of the Palomar emission-line objects range from $\sim 1 \times 10^{40}$ erg s $^{-1}$ for transition objects to $\sim 2 \times 10^{41}$ erg s $^{-1}$ for Seyferts (Table 2). If this emission is produced by a canonical optically thick, physically thin disk, which radiates at $L_{\text{acc}} = \eta \dot{M} c^2 = 5.7 \times 10^{45} (\eta/0.1) (\dot{M}/M_{\odot} \text{ yr}^{-1})$ erg s $^{-1}$, we expect typical mass accretion rates of $\dot{M} \approx 2 \times 10^{-6}$ to $4 \times 10^{-5} M_{\odot} \text{ yr}^{-1}$. These values of \dot{M} are miniscule by comparison with the minimum accretion rates likely to be available through stellar mass loss and Bondi accretion alone. The majority of the Palomar AGNs are hosted by early-type disk galaxies (S0s and Sa–Sbc spirals; see Ho et al. 1997b, 2003a), whose bulges tend to have cuspy light profiles of the “power-law” type. As discussed in § 4.1, the inner regions of such bulges should have $\dot{M}_{*} \approx 10^{-5} - 10^{-3} M_{\odot} \text{ yr}^{-1}$, and probably closer to the upper end of this range because of the additional contribution from central star clusters, which add $\dot{M}_{*} \approx 10^{-3} M_{\odot} \text{ yr}^{-1}$. We have also erred on the side of caution by assuming that all of the stars are old. In actuality, the central regions of many spirals in the Palomar sample often show evidence for some contribution from composite populations (Ho et al. 2009), which will help to boost the mass loss rates even further. Bondi accretion of hot gas contributes roughly the same amount as stellar mass loss, $\dot{M}_{\text{B}} \approx 10^{-5} - 10^{-3} M_{\odot} \text{ yr}^{-1}$. Thus, $\dot{M}_{\text{tot}} = \dot{M}_{*} + \dot{M}_{\text{B}} \approx 10^{-5} - 10^{-3} M_{\odot} \text{ yr}^{-1}$, but more likely, $\dot{M}_{\text{tot}} \gtrsim 10^{-3} M_{\odot} \text{ yr}^{-1}$.

A similar exercise leads to an even stronger result for the absorption-line nuclei, which are found predominantly in elliptical and S0 galaxies. Here, the median L_{bol} of 2×10^{39} erg s $^{-1}$ requires only $\dot{M} \approx 4 \times 10^{-7} M_{\odot} \text{ yr}^{-1}$ for $\eta = 0.1$. On the other hand, the centers of the host galaxies can supply at least $\dot{M}_{*} \approx 10^{-6} - 10^{-4} M_{\odot} \text{ yr}^{-1}$ for low-density cores, a factor of 10 higher still in \dot{M}_{*} for power-law cusps, and yet another 10-fold increase for \dot{M}_{B} . Ho et al. (2003b) highlighted the acuteness of the luminosity-deficit problem for the nearest of the absorption-line objects, M32, whose $2.5 \times 10^6 M_{\odot}$ BH emits merely 9.4×10^{35} erg s $^{-1}$ in the 2–10 keV band at an Eddington ratio of $\sim 3 \times 10^{-9}$.

These simple comparisons suggest that if η indeed is 0.1, then nearby galactic nuclei are 1–4 orders of magnitude underluminous. For the accretion rates that we infer to be present, they should radiate far more prodigiously than actually observed. There are four possible interpretations of this finding. (1) First, our estimates of \dot{M}_{tot} could be too high by a large factor, namely 1–4 orders of magnitude. We consider this to be unlikely. Recall that \dot{M}_{tot} includes only normal mass loss from evolved stars and Bondi accretion of hot gas, either one of which alone would violate the luminosity limit for $\eta = 0.1$; we have conservatively neglected other potential sources of fuel (§ 4.3). (2) Second, it could be argued that perhaps the gas released through stellar mass loss manages to escape from the nucleus before it gets accreted. In actively star-forming galaxies, for example, the collective effects of strong winds and shocks from massive stars can expel gas to large galactocentric distances. This mechanism of gas removal, however, appears to be extremely implausible given the typical ages of the nuclear stellar population (Ho et al. 2003a). Storing the gas in an inert cold disk or converting it to young stars violates other observational constraints (Ho 2008). (3) Third, η may be $\ll 0.1$, as expected from RIAFs (Narayan et al. 1998; Quataert 2001). This is an argument that is frequently invoked to explain the apparent con-

flict between the nuclear luminosities and Bondi accretion rates in some early-type galaxies (e.g., Fabian & Rees 1995; Mahadevan 1997; Di Matteo et al. 2000, 2001; Loewenstein et al. 2001; Ho et al. 2003b). (4) Lastly, an inherent ambiguity exists between inefficient radiation and inefficient accretion. A variety of physical effects, summarized in Ho (2008), can divert the inflowing gas and severely curtail the amount of material that ultimately gets accreted. For instance, if RIAFs naturally develop outflows or winds, as recently shown in a number of studies (see Quataert 2001), the actual accretion rate would be much lower than that estimated at large radii. If so, then η may not need to be so exceptionally low, although it should still be substantially below 0.1 because the outflow models ultimately rely on the accreting gas to be radiatively inefficient. Energy feedback from the AGN, associated with either disk outflows or small-scale radio jets—a ubiquitous feature of low- $L_{\text{bol}}/L_{\text{Edd}}$ systems (Ho 2002a)—may be another culprit for interrupting smooth mass inflow. Ho (2009) presents quantitative evidence that AGN feedback injects nongravitational perturbations to the kinematics of the ionized gas in the Palomar sources.

5.2. Accretion States of Massive Black Holes

By analogy with stellar BHs in X-ray binaries, supermassive BHs in galactic nuclei may evolve through different evolutionary phases, corresponding to distinct “states” (Narayan et al. 1998). The basic physical picture is that the structure of the accretion flow changes in response to variations in the accretion rate. Parameterizing the accretion rate in terms of the dimensionless variable \dot{m} , one can define three, possibly four regimes. (1) When $\dot{m} \gtrsim 1$, an object is in the “very high” state. The high radiation density in these “super-Eddington” sources traps the photons, and the accretion flow is that of an optically thick RIAF or slim disk (Begelman & Meier 1982; Abramowicz et al. 1988). An extragalactic analog of such systems are the narrow-line Seyfert 1 nuclei (Pounds & Vaughan 2000). (2) Objects satisfying $\dot{m}_{\text{crit}} < \dot{m} < 1$ correspond to those in the “high” state. These contain traditionally studied optically thick, geometrically thin, radiatively efficient Shakura & Sunyaev (1973) disks, which are present in classical, relatively luminous Seyfert nuclei and quasars. (3) When $\dot{m} \leq \dot{m}_{\text{crit}}$, an optically thin, geometrically thick, radiatively inefficient flow develops, and the luminosity of the source plummets. Depending on how low the accretion rate drops, one might distinguish between objects in the “low” state ($10^{-6} \leq \dot{m} \leq \dot{m}_{\text{crit}}$) versus those in the “quiescent” state ($\dot{m} < 10^{-6}$). Objects in quiescence are those dominated by, or which exclusively contain, a pure RIAF, such as the Galactic center source Sgr A*. Low-state objects contain a hybrid structure consisting of an inner RIAF plus an outer thin disk, whose truncation radius recedes as \dot{m} decreases. Such a configuration has been suggested for a number of low-luminosity AGNs, especially LINERs (Lasota et al. 1996; Quataert et al. 1999; Ho et al. 2000; Ho 2002b, 2008). We note that the boundary between the low and quiescent states ($\dot{m} \approx 10^{-6}$) is purely illustrative; it remains to be demonstrated that there are two distinct states, and if so, where the transition truly lies.

If AGN activity is characterized by distinct states, as schematically sketched above, then this ought to be reflected in the observed distribution of accretion rates for AGNs spanning the full range of \dot{m} . Since it is difficult to measure \dot{m} directly, $L_{\text{bol}}/L_{\text{Edd}}$ can be used as a surrogate for \dot{m} . We stress, however, that analysis of this kind is only meaningful when performed on

large, well-defined, statistically complete samples. It is dangerous to combine samples with different selection criteria (e.g., Marchesini et al. 2004; Hopkins et al. 2006). With this in mind, we recall that the distribution of $L_{\text{bol}}/L_{\text{Edd}}$ for the entire Palomar sample (Figs. 1*b* and 3*b*)—a more or less complete census of nearby galaxies—shows no obvious substructure that might be identified with physically distinct populations. Unfortunately, the volume sampled by the Palomar survey does not contain sufficient luminous AGNs to properly cover the upper end of the $L_{\text{bol}}/L_{\text{Edd}}$ distribution. This would be an important goal for future statistical studies of AGNs.

6. SUMMARY

Nearly all of the objects in the Palomar survey of nearby galaxies now have central stellar velocity dispersions, from which BH masses can be inferred using the $M_{\text{BH}}-\sigma_*$ relation. A previously published collection of $H\alpha$ line fluxes, in combination with a newly assembled database of nuclear X-ray measurements and a reevaluation of the appropriate bolometric corrections, provides estimates of the accretion luminosity of the nuclei. We use these resources to evaluate the distribution of bolometric luminosities and Eddington ratios for a large, well-defined sample of galactic nuclei in order to investigate the nature of accretion onto massive BHs in nearby galaxies.

Nearby galactic nuclei span at least 7 orders of magnitude in nuclear bolometric luminosities, from $L_{\text{bol}} < 10^{37}$ to $\sim 3 \times 10^{44}$ erg s⁻¹, and an even broader range in Eddington ratios, from $L_{\text{bol}}/L_{\text{Edd}} \approx 10^{-9}$ to 10^{-1} . Both L_{bol} and $L_{\text{bol}}/L_{\text{Edd}}$, but especially the latter, decrease systematically along the following spectral sequence: Seyferts → LINERs → transition objects → absorption-line nuclei. The spectral diversity of emission-line nuclei reflects and is primarily controlled by variations in the mass accretion rate. The characteristic value of $L_{\text{bol}}/L_{\text{Edd}}$ also varies systematically along the Hubble sequence, increasing from galaxies with large to small bulge-to-disk ratios.

The accretion rates inferred from the nuclear luminosities, assuming a standard radiative efficiency of $\eta = 0.1$, are very low, typically $\dot{M} \lesssim 10^{-6}$ to $10^{-5} M_{\odot} \text{ yr}^{-1}$. Such tiny rates can easily be supplied *in situ* by ordinary mass loss from evolved stars in the nuclear stellar cusp or central star clusters, or by Bondi accretion of hot gas in the inner bulges of galaxies detected in X-ray observations. Indeed, we argue that conservative estimates of the gas mass potentially available for accretion already far exceed the observational limits imposed by the luminosity measurements, suggesting that in many, if not most, nearby galaxies the radiative efficiency is likely to be much less than 0.1. The requirement for exceptionally low radiative efficiencies, however, could be mitigated if the actual accretion rates are curtailed by AGN feedback in the form of disk outflows or small-scale radio jets. The prevalence of RIAFs is further supported by the low Eddington ratios: all the objects in our sample are sub-Eddington systems, with the majority having values of $L_{\text{bol}}/L_{\text{Edd}}$ that satisfy the theoretically predicted criterion for RIAFs.

We suggest that massive BHs in galactic nuclei evolve through distinct states in response to changes in the mass accretion rate. The nearby objects considered in this study are largely systems in the low or quiescent state. We see no evidence of bimodality in the distribution of $L_{\text{bol}}/L_{\text{Edd}}$, but this is probably a consequence of the limited volume probed by the Palomar survey. It would be of considerable interest to extend the analysis presented here to include objects of higher luminosity in order to map out the full distribution of AGN luminosities and Eddington ratios.

This work was supported by the Carnegie Institution of Washington and by *Chandra* grant GO5-6107X. I thank Louis-Benoit Desroches for help with analyzing some of the archival *Chandra* data. An anonymous referee offered a positive and helpful report.

REFERENCES

- Abramowicz, M. A., Czerny, B., Lasota, J.-P., & Szuszkiewicz, E. 1988, *ApJ*, 332, 646
- Allen, A. J., & Hughes, P. A. 1987, *ApJ*, 313, 152
- Armitage, P. J., Zurek, W. H., & Davies, M. B. 1996, *ApJ*, 470, 237
- Athey, A. E., Bregman, J. N., Bregman, J. D., Temi, P., & Sauvage, M. 2002, *ApJ*, 571, 272
- Baganoff, F. K., et al. 2003, *ApJ*, 591, 891
- Begelman, M. C., & Meier, D. L. 1982, *ApJ*, 253, 873
- Blanton, E. L., Sarazin, C. L., & Irwin, J. A. 2001, *ApJ*, 552, 106
- Böker, T., van der Marel, R. P., Laine, S., Rix, H.-W., Sarzi, M., Ho, L. C., & Shields, J. C. 2002, *AJ*, 123, 1389
- Bondi, H. 1952, *MNRAS*, 112, 195
- Cappi, M., et al. 2006, *A&A*, 446, 459
- Carollo, C. M., Stiavelli, M., de Zeeuw, P. T., & Mack, J. 1997, *AJ*, 114, 2366
- Carswell, R. F., Baldwin, J. A., Atwood, B., & Phillips, M. M. 1984, *ApJ*, 286, 464
- Chokshi, A., & Turner, E. L. 1992, *MNRAS*, 259, 421
- Ciotti, L., D’Ercole, A., Pellegrini, S., & Renzini, A. 1991, *ApJ*, 376, 380
- Dahlem, M., & Stuhmann, N. 1998, *A&A*, 332, 449
- Deluit, S., & Courvoisier, T. J.-L. 2003, *A&A*, 399, 77
- Desroches, L.-B., & Ho, L. C. 2009, *ApJ*, 690, 267
- Di Matteo, T., Johnstone, R. M., Allen, S. W., & Fabian, A. C. 2001, *ApJ*, 550, L19
- Di Matteo, T., Quataert, E., Allen, S. W., Narayan, R., & Fabian, A. C. 2000, *MNRAS*, 311, 507
- Dudík, R. P., Satyapal, S., Gliozzi, M., & Sambruna, R. M. 2005, *ApJ*, 620, 113
- Edwards, A. C. 1980, *MNRAS*, 190, 757
- Elvis, M., et al. 1994, *ApJS*, 95, 1
- Eracleous, M., Shields, J. C., Chartas, G., & Moran, E. C. 2002, *ApJ*, 565, 108
- Faber, S. M., & Gallagher, J. S. 1976, *ApJ*, 204, 365
- Faber, S. M., et al. 1997, *AJ*, 114, 1771
- Fabian, A. C., & Canizares, C. R. 1988, *Nature*, 333, 829
- Fabian, A. C., & Rees, M. J. 1995, *MNRAS*, 277, L55
- Fanaroff, B. L., & Riley, J. M. 1974, *MNRAS*, 167, 31P
- Feigelson, E. D., & Nelson, P. I. 1985, *ApJ*, 293, 192
- Ferrarese, L., & Merritt, D. 2000, *ApJ*, 539, L9
- Ferrarese, L., et al. 2006, *ApJS*, 164, 334
- Filippenko, A. V., & Ho, L. C. 2003, *ApJ*, 588, L13
- Flohic, H. M. L. G., Eracleous, M., Chartas, G., Shields, J. C., & Moran, E. C. 2006, *ApJ*, 647, 140
- Frank, J. 1978, *MNRAS*, 184, 87
- Frank, J., King, A. R., & Raine, D. J. 1992, *Accretion Power in Astrophysics* (Cambridge: Cambridge Univ. Press)
- Fukazawa, Y., Iyomoto, N., Kubota, A., Matsumoto, Y., & Makishima, K. 2001, *A&A*, 374, 73
- Fukugita, M., Shimasaku, K., & Ichikawa, T. 1995, *PASP*, 107, 945
- Garcia, M. R., Williams, B. F., Yuan, F., Kong, A. K. H., Primini, F. A., Barmby, P., Kaaret, P., & Murray, S. S. 2005, *ApJ*, 632, 1042
- Gebhardt, K., et al. 2000, *ApJ*, 539, L13
- González-Martín, O., Masegosa, J., Márquez, I., Guerrero, M. A., & Dultzin-Hacyan, D. 2006, *A&A*, 460, 45
- Greene, J. E., & Ho, L. C. 2004, *ApJ*, 610, 722
- . 2005, *ApJ*, 630, 122
- . 2007a, *ApJ*, 667, 131
- . 2007b, *ApJ*, 670, 92
- Halderson, E. L., Moran, E. C., Filippenko, A. V., & Ho, L. C. 2001, *AJ*, 122, 637
- Halpern, J. P., Eracleous, M., Filippenko, A. V., & Chen, K. 1996, *ApJ*, 464, 704
- Hills, J. G. 1975, *Nature*, 254, 295
- Ho, L. C. 1999a, in *Observational Evidence for Black Holes in the Universe*, ed. S. K. Chakrabarti (Dordrecht: Kluwer), 157
- . 1999b, *ApJ*, 516, 672
- . 2002a, *ApJ*, 564, 120
- . 2002b, in *Issues in Unification of AGNs*, ed. R. Maiolino, A. Marconi, & N. Nagar (San Francisco, CA: ASP), 165

- . 2008, *ARA&A*, 46, 475
- . 2009, *ApJ*, in press
- Ho, L. C., Filippenko, A. V., & Sargent, W. L. W. 1996, *ApJ*, 462, 183
- . 1997a, *ApJS*, 112, 315
- . 1997b, *ApJ*, 487, 568
- . 1997c, *ApJ*, 487, 591
- . 2003a, *ApJ*, 583, 159
- Ho, L. C., Greene, J. E., Filippenko, A. V., & Sargent, W. L. W. 2009, *ApJS*, in press
- Ho, L. C., Rudnick, G., Rix, H.-W., Shields, J. C., McIntosh, D. H., Filippenko, A. V., Sargent, W. L. W., & Eracleous, M. 2000, *ApJ*, 541, 120
- Ho, L. C., Terashima, Y., & Ulvestad, J. S. 2003b, *ApJ*, 589, 783
- Ho, L. C., et al. 2001, *ApJ*, 549, L51
- Hopkins, P. F., Narayan, R., & Hernquist, L. 2006, *ApJ*, 643, 641
- Huchra, J. P., & Burg, R. 1992, *ApJ*, 393, 90
- Irwin, J. A., Sarazin, C. L., & Bregman, J. N. 2002, *ApJ*, 570, 152
- Iwasawa, K., Fabian, A. C., & Matt, G. 1997a, *MNRAS*, 289, 443
- Iwasawa, K., Fabian, A. C., Ueno, S., Awaki, H., Matsushita, K., & Makishima, K. 1997b, *MNRAS*, 285, 683
- Jungwiert, B., Combes, F., & Palous, J. 2001, *A&A*, 376, 85
- Komossa, S., Böhringer, H., & Huchra, J. P. 1999, *A&A*, 349, 88
- Kormendy, J. 2004, in *Carnegie Observatories Astrophysics Series, Vol. 1: Coevolution of Black Holes and Galaxies*, ed. L. C. Ho (Cambridge: Cambridge Univ. Press), 1
- Kormendy, J., Fisher, D. B., Cornell, M. E., & Bender, R. 2009, *ApJS*, in press
- Lasota, J.-P., Abramowicz, M. A., Chen, X., Krolik, J., Narayan, R., & Yi, I. 1996, *ApJ*, 462, 142
- Lauer, T. R., Faber, S. M., Ajhar, E. A., Grillmair, C. J., & Scowen, P. A. 1998, *AJ*, 116, 2263
- Lauer, T. R., et al. 1995, *AJ*, 110, 2622
- Liu, J.-F., & Bregman, J. N. 2005, *ApJS*, 157, 59
- Loewenstein, M., Mushotzky, R. F., Angelini, L., Arnaud, K. A., & Quataert, E. 2001, *ApJ*, 555, L21
- Magorrian, J., et al. 1998, *AJ*, 115, 2285
- Mahadevan, R. 1997, *ApJ*, 477, 585
- Maizumi, D. 2007, *MNRAS*, 377, 1696
- Marchesini, D., Celotti, A., & Ferrarese, L. 2004, *MNRAS*, 351, 733
- Mathews, W. G. 1990, *ApJ*, 354, 468
- McLure, R. J., & Dunlop, J. S. 2004, *MNRAS*, 352, 1390
- Milosavljević, M., Merritt, D., & Ho, L. C. 2006, *ApJ*, 652, 120
- Narayan, R., Mahadevan, R., & Quataert, E. 1998, in *The Theory of Black Hole Accretion Discs*, ed. M. A. Abramowicz, G. Björnsson, & J. E. Pringle (Cambridge: Cambridge Univ. Press), 148
- Narayan, R., & Yi, I. 1994, *ApJ*, 428, L13
- . 1995, *ApJ*, 444, 231
- Padovani, P., & Matteucci, F. 1993, *ApJ*, 416, 26
- Panessa, F., Bassani, L., Cappi, M., Dadina, M., Barcons, X., Carrera, F. J., Ho, L. C., & Iwasawa, K. 2006, *A&A*, 455, 173
- Pappa, A., Georgantopoulos, I., Stewart, G. C., & Zezas, A. L. 2001, *MNRAS*, 326, 995
- Parriott, J. R., & Bregman, J. N. 2008, *ApJ*, 681, 1215
- Pellegrini, S. 2005, *ApJ*, 624, 155
- Pellegrini, S., Siemiginowska, A., Fabbiano, G., Elvis, M., Greenhill, L., Soria, R., Baldi, A., & Kim, D. W. 2007, *ApJ*, 667, 749
- Pfefferkorn, F., Boller, Th., & Rafanelli, P. 2001, *A&A*, 368, 797
- Phillips, A. C., Illingworth, G. D., MacKenty, J. W., & Franx, M. 1996, *AJ*, 111, 1566
- Pounds, K. A., & Vaughan, S. 2000, *New Astron. Rev.*, 44, 411
- Quataert, E. 2001, in *Probing the Physics of Active Galactic Nuclei by Multiwavelength Monitoring*, ed. B. M. Peterson, R. S. Polidan, & R. W. Pogge (San Francisco, CA: ASP), 71
- Quataert, E., Di Matteo, T., Narayan, R., & Ho, L. C. 1999, *ApJ*, 525, L89
- Rauch, K. P. 1999, *ApJ*, 514, 725
- Ravindranath, S., Ho, L. C., Peng, C. Y., Filippenko, A. V., & Sargent, W. L. W. 2001, *AJ*, 122, 653
- Rees, M. J. 1988, *Nature*, 333, 523
- Rest, A., van den Bosch, F. C., Jaffe, W., Tran, H., Tsvetanov, Z., Ford, H. C., Davies, J., & Schafer, J. 2001, *AJ*, 121, 2431
- Reynolds, C. S., Nowak, M. A., Markoff, S., Tueller, J., Wilms, J., & Young, A. J. 2009, *ApJ*, 691, 1159
- Roberts, T. P., & Warwick, R. S. 2000, *MNRAS*, 315, 98
- Sansom, A. E., O'Sullivan, E., Forbes, D. A., Proctor, R. N., & Davis, D. S. 2006, *MNRAS*, 370, 1541
- Sarazin, C., Irwin, J. A., & Bregman, J. N. 2000, *ApJ*, 544, L101
- Sarzi, M., et al. 2005, *ApJ*, 628, 169
- Satyapal, S., Dudik, R. P., O'Halloran, B., & Gliozzi, M. 2005, *ApJ*, 633, 86
- Satyapal, S., Sambruna, R. M., & Dudik, R. P. 2004, *A&A*, 414, 825
- Schmitt, H. R. 2001, *AJ*, 122, 2243
- Scoville, N., & Norman, C. 1988, *ApJ*, 332, 163
- Shakura, N. I., & Sunyaev, R. A. 1973, *A&A*, 24, 337
- Shirey, R., et al. 2001, *A&A*, 365, L195
- Shuder, J. M., & Osterbrock, D. E. 1981, *ApJ*, 250, 55
- Sivakoff, G. R., Sarazin, C. L., & Irwin, J. A. 2003, *ApJ*, 599, 218
- Soldatenkov, D., Vikhlinin, A., & Pavlinsky, M. 2003, *Astron. Lett.*, 5, 298
- Sołtan, A. 1982, *MNRAS*, 200, 115
- Soria, R., Fabbiano, G., Graham, A., Baldi, A., Elvis, M., Jerjen, H., Pellegrini, S., & Siemiginowska, A. 2006, *ApJ*, 640, 126
- Spitzer Jr., L., & Saslaw, W. C. 1966, *ApJ*, 143, 400
- Storchi-Bergmann, T., Baldwin, J. A., & Wilson, A. S. 1993, *ApJ*, 410, L11
- Swartz, D. A., Ghosh, K. K., McCollough, M. L., Pannuti, T. G., Tennant, A. F., & Wu, K. 2003, *ApJS*, 144, 213
- Terashima, Y., Iyomoto, N., Ho, L. C., & Ptak, A. F. 2002, *ApJS*, 139, 1
- Terashima, Y., & Wilson, A. S. 2003, *ApJ*, 583, 145
- Tremaine, S., et al. 2002, *ApJ*, 574, 740
- Vasudevan, R. V., & Fabian, A. C. 2007, *MNRAS*, 381, 1235
- Voit, G. M., & Shull, J. M. 1988, *ApJ*, 331, 197
- Wada, K. 2004, in *Carnegie Observatories Astrophysics Series, Vol. 1: Coevolution of Black Holes and Galaxies*, ed. L. C. Ho (Cambridge: Cambridge Univ. Press), 186
- Wrobel, J. M., Terashima, Y., & Ho, L. C. 2008, *ApJ*, 675, 1041
- Zhang, Y., Gu, Q.-S., & Ho, L. C. 2008, *A&A*, 487, 177

APPENDIX

NUCLEAR X-RAY LUMINOSITIES

This Appendix summarizes the X-ray luminosities used in this paper. We performed a comprehensive literature search of all published X-ray measurements for the AGNs (Seyferts, LINERs, and transition objects) and absorption-line nuclei in the Palomar survey. Because of the faintness of most nearby nuclei and potential confusion with circumnuclear emission, the most crucial consideration is angular resolution. With a point-spread function (PSF) of FWHM $\approx 1''$ and low background noise, the instrument of choice is ACIS on *Chandra*. Although less ideal, the HRI imager on *ROSAT* and the MOS camera on *XMM-Newton*, both having PSFs with FWHM $\approx 5''$, also yield acceptable data under most circumstances. For sources bright enough for rigorous spectral analysis, even lower resolution observations (e.g., *ASCA*) can be used if the nucleus can be isolated through spectral fitting.

Of the 277 galaxies in the parent sample, acceptable literature data were located for 166. Most of the observations (75%) were acquired with *Chandra*/ACIS, and the rest were taken largely with *ROSAT*/HRI or *XMM-Newton*. Only a small handful come from *ROSAT*/PSPC and *ASCA*; one object was observed with *BeppoSAX*. We also performed a thorough search of the *Chandra* archives and included all useful, unpublished data that were nonproprietary as of 2007 October. A total of nine additional galaxies were located. We analyzed these data sets following standard techniques, as described in Ho et al. (2001) and Desroches & Ho (2009).

Table 3 lists X-ray luminosities for the final sample of 175 galaxies. Because the literature data were acquired with a variety of different instruments and analyzed using many different techniques, we converted all the luminosities to one standard bandpass, 2–10 keV. When reliable spectral fits are available, we use the published best-fit spectral slope to extrapolate to the desired bandpass. Otherwise, we assume a photon index of $\Gamma = 1.8$, which is close to the typical values observed in low-luminosity AGNs (see Ho 2008, and references therein). Likewise, we quote intrinsic (absorption-corrected) luminosities whenever possible. Although many of the fainter sources do not have sufficient counts to constrain the absorbing column, many lines of evidence suggest that most low-luminosity AGNs do not suffer from much obscuration (Ho 2008).

TABLE 3
NUCLEAR X-RAY LUMINOSITIES

Galaxy (1)	D_L (Mpc) (2)	$\log(L_X/\text{erg s}^{-1})$ (3)	Tel. (4)	Ref. (5)	Galaxy (1)	D_L (Mpc) (2)	$\log(L_X/\text{erg s}^{-1})$ (3)	Tel. (4)	Ref. (5)
IC 239	16.8	<38.05	C	1	NGC 2775	17.0	39.07	R	18
IC 1727	8.2	<37.92	C	2	NGC 2787	13.0	38.79	C	13
NGC 147	0.7	<36.18	R	3	NGC 2832	91.6	<41.49	R	22
NGC 185	0.7	<35.92	R	4	NGC 2841	12.0	38.26	C	13
NGC 205	0.7	<36.41	R	3	NGC 3031	1.4	39.38	C	13
NGC 221	0.7	35.85	C	5	NGC 3079	20.4	38.60	C	14
NGC 224	0.7	35.85	C	6	NGC 3115	6.7	38.41	C	2
NGC 266	62.4	40.88	C	7	NGC 3147	40.9	41.87	C	7
NGC 315	65.8	41.63	C	8	NGC 3169	19.7	41.05	C	7
NGC 404	2.4	37.02	C	9	NGC 3185	21.3	38.99	X	11
NGC 410	70.6	40.09	C	1	NGC 3190	22.4	39.54	R	3
NGC 474	32.5	<38.36	C	1	NGC 3193	23.2	<39.41	R	3
NGC 507	65.7	40.66	C	2	NGC 3226	23.4	39.99	C	8
NGC 628	9.7	38.14	C	2	NGC 3227	20.6	41.70	X	11
NGC 660	11.8	38.55	C	10	NGC 3245	22.2	39.29	C	8
NGC 676	19.5	39.00	X	11	NGC 3368	8.1	39.10	C	14
NGC 821	23.2	39.42	C	12	NGC 3377	8.1	38.24	C	23
NGC 1023	10.5	38.04	C	1	NGC 3379	8.1	37.53	C	8
NGC 1052	17.8	41.53	C	8	NGC 3384	8.1	37.79	C	3
NGC 1055	12.6	<38.19	C	13	NGC 3412	8.1	<37.22	C	1
NGC 1058	9.1	<37.57	C	13	NGC 3486	7.4	37.51	C	13
NGC 1068	14.4	43.63	A	31	NGC 3489	6.4	37.67	C	13
NGC 1167	65.3	40.32	C	15	NGC 3507	19.8	38.30	C	8
NGC 1275	70.1	42.86 ^a	X	16	NGC 3516	38.9	42.39	X	16
NGC 1358	53.6	42.68	B	17	NGC 3607	19.9	38.63	C	8
NGC 1667	61.2	40.55	C	15	NGC 3608	23.4	38.85	C	8
NGC 1961	53.1	40.31	R	3	NGC 3610	29.2	38.79	C	1
NGC 2273	28.4	40.02	R	18	NGC 3623	7.3	38.25	C	14
NGC 2300	31.0	40.93	R	18	NGC 3627	6.6	<37.22	C	13
NGC 2541	10.6	<38.00	C	19	NGC 3628	7.7	38.24	C	8
NGC 2639	42.6	40.85	A	20	NGC 3640	24.2	<38.37	C	1
NGC 2655	24.4	41.87	A	20	NGC 3642	27.5	39.84	R	18
NGC 2681	13.3	38.72	C	8	NGC 3675	12.8	<37.98	C	13
NGC 2683	5.7	38.01	C	19	NGC 3718	17.0	40.44	C	19
NGC 2685	16.2	39.90	X	11	NGC 3884	91.6	41.89	C	24
NGC 2768	23.7	40.59	R	21	NGC 3898	21.9	<38.82	C	21

TABLE 3—*Continued*

Galaxy (1)	D_L (Mpc) (2)	$\log(L_X/\text{erg s}^{-1})$ (3)	Tel. (4)	Ref. (5)	Galaxy (1)	D_L (Mpc) (2)	$\log(L_X/\text{erg s}^{-1})$ (3)	Tel. (4)	Ref. (5)
NGC 3941	18.9	39.27	X	11	NGC 4435	16.8	39.60	R	18
NGC 3982	17.0	38.76	C	16	NGC 4438	16.8	39.21	C	8
NGC 3998	21.6	41.34	R	3	NGC 4450	16.8	40.02	C	21
NGC 4013	17.0	<37.57	C	10	NGC 4457	17.4	39.05	C	8
NGC 4036	24.6	39.96	R	18	NGC 4459	16.8	38.87	C	8
NGC 4051	17.0	42.07	C	14	NGC 4472	16.8	<38.69	C	26
NGC 4111	17.0	39.33	C	8	NGC 4473	16.8	<38.20	C	1
NGC 4125	24.2	38.94	C	8	NGC 4477	16.8	39.60	X	11
NGC 4138	17.0	40.11	C	11	NGC 4478	16.8	<39.08	C	27
NGC 4143	17.0	40.03	C	7	NGC 4486	16.8	40.78 ^a	C	8
NGC 4150	9.7	<37.13	C	19	NGC 4494	9.7	39.12	C	8
NGC 4151	20.3	43.07	C	14	NGC 4501	16.8	38.89	C	19
NGC 4168	16.8	<38.24	C	16	NGC 4527	13.5	38.80	C	10
NGC 4192	16.8	39.58	A	20	NGC 4548	16.8	39.74	C	7
NGC 4203	9.7	39.69	C	13	NGC 4550	16.8	<38.42	C	7
NGC 4216	16.8	38.91	C	1	NGC 4552	16.8	39.49	C	8
NGC 4235	35.1	42.25	X	16	NGC 4564	16.8	39.12	C	23
NGC 4251	9.7	<37.78	C	1	NGC 4565	9.7	39.56	C	7
NGC 4258	6.8	40.89	X	34	NGC 4569	16.8	39.41	C	13
NGC 4261	35.1	40.59 ^a	C	8	NGC 4579	16.8	41.15	C	8
NGC 4278	9.7	39.64	C	13	NGC 4594	20.0	40.69	C	8
NGC 4291	29.4	40.63	R	18	NGC 4596	16.8	38.65	C	8
NGC 4293	17.0	<39.37	C	4	NGC 4621	16.8	38.85	C	28
NGC 4314	9.7	38.13	C	8	NGC 4636	17.0	39.38	C	8
NGC 4321	16.8	<38.62	C	13	NGC 4638	16.8	<39.11	R	3
NGC 4346	17.0	<39.82	C	4	NGC 4639	16.8	40.18	C	13
NGC 4350	16.8	38.81	C	10	NGC 4649	16.8	38.10	C	29
NGC 4365	16.8	38.00	C	25	NGC 4651	16.8	39.32	R	18
NGC 4374	16.8	39.50 ^a	C	8	NGC 4698	16.8	38.69	C	8
NGC 4382	16.8	37.87	C	25	NGC 4713	17.9	38.40	C	2
NGC 4388	16.8	42.14	A	33	NGC 4725	12.4	39.11	C	13
NGC 4394	16.8	<38.49	R	4	NGC 4736	4.3	38.48	C	8
NGC 4395	3.6	39.58	C	8	NGC 4750	26.1	39.94	C	10
NGC 4406	16.8	40.39	R	18	NGC 4762	16.8	38.26	C	4
NGC 4414	9.7	38.62	C	2	NGC 4772	16.3	39.30	C	4
NGC 4419	16.8	39.08	C	10	NGC 4826	4.1	<37.33	C	13

TABLE 3—*Continued*

Galaxy (1)	D_L (Mpc) (2)	$\log(L_X/\text{erg s}^{-1})$ (3)	Tel. (4)	Ref. (5)	Galaxy (1)	D_L (Mpc) (2)	$\log(L_X/\text{erg s}^{-1})$ (3)	Tel. (4)	Ref. (5)
NGC 5005	21.3	39.94	C	10	NGC 5850	28.5	<39.54	R	3
NGC 5033	18.7	40.70	C	13	NGC 5866	15.3	38.60	C	8
NGC 5055	7.2	38.37	C	8	NGC 6482	52.3	39.36	C	8
NGC 5194	7.7	41.03	B	32	NGC 6500	39.7	39.73	C	7
NGC 5195	9.3	<38.00	C	13	NGC 6503	6.1	37.10	C	14
NGC 5273	21.3	41.61	X	11	NGC 6654	29.5	<39.56	R	3
NGC 5322	31.6	40.26	R	18	NGC 7217	16.0	39.87	R	18
NGC 5353	37.8	<39.29	C	18	NGC 7331	14.3	38.66	C	8
NGC 5354	32.8	<39.63	R	3	NGC 7332	18.2	<39.49	C	27
NGC 5363	22.4	<40.05	X	30	NGC 7457	12.3	37.86	C	1
NGC 5371	37.8	40.84	R	21	NGC 7479	32.4	41.15	X	16
NGC 5548	67.0	43.23	X	16	NGC 7619	50.7	40.80	C	2
NGC 5678	35.6	39.29	C	2	NGC 7626	45.6	40.97	C	2
NGC 5746	29.4	40.28	C	8	NGC 7742	22.2	39.94	R	18
NGC 5813	28.5	38.51	C	27	NGC 7743	24.4	39.71	X	16
NGC 5846	28.5	39.65	C	8					

NOTE.— Col. (1) Galaxy name. Col. (2) Adopted distance. Col. (3) X-ray luminosity in the 2–10 keV band. Col. (4) Telescope: A = *ASCA*; B = *BeppoSAX*; C = *Chandra*/ACIS; R = *ROSAT*/HRI; X = *XMM-Newton*. Col. (5) Reference for the X-ray data: (1) Desroches & Ho (2009); (2) *Chandra* archives, analyzed in this paper; (3) Roberts & Warwick (2000); (4) Halderson et al. (2001); (5) Ho et al. (2003b); (6) Garcia et al. (2005); (7) Terashima & Wilson (2003); (8) González-Martín et al. (2006); (9) Eracleous et al. (2002); (10) Dudik et al. (2005); (11) Cappi et al. (2006); (12) Pellegrini et al. (2007); (13) Ho et al. (2001); (14) Satyapal et al. (2004); (15) Pappa et al. (2001); (16) Panessa et al. (2006); (17) Deluit & Courvoisier (2003); (18) Liu & Bregman (2005); (19) Satyapal et al. (2005); (20) Terashima et al. (2002); (21) Komossa et al. (1999); (22) Dahlem & Stuhmann (1998); (23) Soria et al. (2006); (24) Pfefferkorn et al. (2001); (25) Sivakoff et al. (2003); (26) Loewenstein et al. (2001); (27) Pellegrini (2005); (28) Wrobel et al. (2008); (29) Soldatenkov et al. (2003); (30) Sansom et al. (2006); (31) Iwasawa et al. (1997a); (32) Fukazawa et al. (2001); (33) Iwasawa et al. (1997b); (34) Reynolds et al. (2009).

^aNuclear luminosity possibly contaminated by jet emission.